Journal of Nanobiotechnology

RESEARCH Open Access

Encapsulated *lactiplantibacillus plantarum* improves Alzheimer's symptoms in APP/PS1 mice

Fangfang Hu[1], Qian Gao[1], Caiyun Zheng[1], Wenhui Zhang[1], Ziyi Yang[1], Shihao Wang[1], Yanni Zhang[1*] and Tingli Lu[1*]

Abstract

Background Alzheimer's disease (AD) is a neurodegenerative disorder that can result in neurotoxicity and an imbalance in gut microbiota. Probiotics have been shown to play an important role in regulating the gut microbiota, but their viability and bioactivity are often compromised as they traverse the gastrointestinal tract, thereby reducing their efficacy and limiting their clinical utility.

Results In this work, layer-by-layer (LbL) encapsulation technology was used to encapsulate *Lactiplantibacillus plantarum* (LP) to improve the above shortcomings. Studies in APPswe/PS1dE9 (APP/PS1) transgenic mice show that LbL-encapsulated LP ($(CS/SP)_2$-LP) protects LP from gastrointestinal damage while $(CS/SP)_2$-LP treatment It improves brain neuroinflammation and neuronal damage in AD mice, reduces Aβ deposition, improves tau protein phosphorylation levels, and restores intestinal barrier damage in AD mice. In addition, post-synaptic density protein 95 (PSD-95) expression increased in AD mice after treatment, indicating enhanced synaptic plasticity. Fecal metabolomic and microbiological analyzes showed that the disordered intestinal microbiota composition of AD mice was restored and short-chain fatty acids (SCFAs) levels were significantly increased after $(CS/SP)_2$-LP treatment.

Conclusion Overall, the above evidence suggests that $(CS/SP)_2$-LP can improve AD symptoms by restoring the balance of intestinal microbiota, and $(CS/SP)_2$-LP treatment will provide a new method to improve the symptoms of AD patients.

Keywords Alzheimer's disease, APP/PS1 mice, *Lactiplantibacillus plantarum*, Layer-by-layer, Gut Microbiome, Short-chain fatty acids

*Correspondence:
Yanni Zhang
yann.zhang@nwpu.edu.cn
Tingli Lu
lutinglixinxin@nwpu.edu.cn
[1]Key Laboratory of Space Bioscience and Biotechnology, Engineering Research Center of Chinese Ministry of Education for Biological Diagnosis, Treatment and Protection Technology and Equipment, School of Life Sciences, Northwestern Polytechnical University, Xi'an 710072, P. R. China

Introduction

Alzheimer's disease (AD) is a progressive neurodegenerative disorder [1], clinically characterized by cognitive decline and progressive memory loss [2]. AD has affected about 30–35 million people worldwide [3]. The increasing prevalence of AD due to longer life expectancy has become a significant health problem and economic burden on society. It is projected that by 2030, around 78 million people will be afflicted with AD. The pathogenesis of AD is complex, with the amyloid hypothesis and the Tau protein hypothesis being the main current theories [4]. However, numerous clinical trials investigating both hypotheses have been terminated, indicating an urgent need for new therapeutic strategies [1].

Bidirectional communication between the gut microbiota and the brain occurs through immune, circulatory, and neural pathways known as the gut-brain axis (GBA). A growing body of evidence emphasizes the role of the gut microbiota and its metabolites in AD development [5]. Dysregulation of gut ecology plays a vital role in the pathogenesis central nervous system (CNS)–related diseases [6]. For example, the loss of commensal bacteria in the gut affects the immune response and disrupts colonization resistance against potential pathogens [7]. Gut microbes indirectly communicate with the CNS by producing several neuroactive metabolites, such as short-chain fatty acids (SCFAs), branched-chain amino acids, lipopolysaccharides (LPS), cholipopolysaccharides, and catecholamines, which synthesize neurotransmitters with neuromodulatory properties [6].

Strategies such as prebiotic intake, probiotics, and fecal microbiota transplantation (FMT) may positively impact cognitive function in AD patients by modulating the gut microbiota. FMT treatment has been reported to improve cognitive deficits and reduce brain deposition of amyloid-β (Aβ) in APPswe/PS1dE9 (APP/PS1) transgenic mice. These beneficial effects were associated with the reversal of changes in gut microbiota and SCFAs, suggesting that FMT treatment may be a potential therapeutic strategy for AD [8]. Oligofructose has also been found to ameliorate cognitive deficits and neurodegeneration in APP/PS1 transgenic mice by modulating the gut microbiota [9]. Regulation of the probiotic *Clostridium butyricum* significantly ameliorates cognitive deficits, microglia activation, neurodegeneration, and Aβ deposition by modulating abnormal gut microbes and the metabolite butyric acid [10]. Furthermore, *Bifidobacterium* has been shown to improve brain function in $A\beta_{1\text{-}42}$-treated mice by modulating the gut microbiome [11]. A probiotic preparation consisting of *Bifidobacterium lactis*, *Lactobacillus casei*, *Bifidobacterium bifidum*, and *Lactobacillus acidophilus* demonstrated a reversal of cognitive deficits after 12 weeks of treatment in SAMP8 (senescence-accelerated mice prone 8) mice [12].

Probiotics can potentially alter brain function through direct and/or indirect multimodal effects, including the endocrine system, parasympathetic autonomic system (e.g. vagus), and immune systems [13]. Probiotics improve intestinal and immune homeostasis by restoring the gut microbiota and exhibit neuroprotective effects in CNS disease by enhancing the production of neurotransmitters such as glutamate and γ-aminobutyric acid (GABA), as well as increasing brain-derived neurotrophic factor (BDNF) levels [14, 15]. Recent studies have shown that *Lactiplantibacillus plantarum* (LP) improves cognitive impairment in 5XFAD and aged mice by regulating NF-κB-mediated BDNF expression. It was also found that treatment with LP can alleviate intestinal barrier damage and inhibit microglial activation. Therefore, increasing the abundance of LP in the intestine is of great significance for the treatment and intervention of AD. However, probiotics are severely destroyed by gastric acid, digestive enzymes and bile salts in the gastrointestinal tract and competition from other bacteria resulted in a significant decrease in the activity of probiotics. In addition, the rapid gastrointestinal (GI) transit time also makes it difficult for probiotics to remain and colonize in the intestine [16–18]. These factors make it challenging for probiotics to effectively exert their therapeutic effects. Therefore, finding a way to quickly deliver LP to the intestine to increase its abundance in the intestines of AD mice is a current challenge.

The layer-by-layer (LbL) encapsulation strategy offers significant flexibility in designing probiotic-based delivery systems. Oppositely charged polyelectrolytes can from multilayer capsules through electrostatic interactions [19]. This method supports the direct adhesion, growth and proliferation of probiotics on the intestinal surface, and the entire encapsulation process can be carried out under mild conditions [20, 21]. Natural polysaccharides such as chitosan (CS), pectin and alginate are favorable for developing macro/nano formulations that protect active substances from the harsh conditions of the gastrointestinal tract [22, 23]. Additionally, numerous studies have shown that polysaccharides can be fermented by the intestinal microbiota, exerting prebiotic effects and promoting health [24–26]. CS is widely used due to its good biocompatibility and unique adhesion properties. Sodium phytate (SP), derived from natural sources such as plant bran and seeds, is known for its excellent biosafety and is commonly used as a food additive [27]. In this study, we aimed to investigate the effects of CS/SP encapsulation on LP survival in the gastrointestinal tract and its intestinal adhesion, as well as to explore the impact of increased LP abundance on cognition in AD mice. Finally, we sought to elucidate the relationship between gut microbiota modulation and the anti-AD effects of $(CS/SP)_2$-LP in AD mice.

Materials and methods

Materials and antibodies

Chitosan (Mw = 100,000-300,000 Da, CS) was purchased from Sigma-Aldrich, sodium phytate (SP) was obtained from Macklin (Shanghai, China), simulated gastric fluid (SGF) and simulated intestinal fluid (SIF) was purchased from Coolaber (Beijing, China), fluorescein isothiocyanate (FITC) was purchased from Dogesce (Beijing, China), man Rogosa Sharpe (MRS) broth was purchased from HKM (Guangzhou, China), and *Lactiplantibacillus plantarum* ATCC8014 (LP) was obtained from Beijing Kizhan (Beijing, China).

Animals

Six-month-old transgenic mice APP/PS1 and wild C57BL/6J were purchased from Beijing Huafukang Biotechnology Co. (Beijing, China). All mice were raised under standard specific pathogen-free (SPF) conditions at 23 ± 2℃, with 40-70% air humidity and a 12-hour light/dark cycle. The animal experiment was approved by the Animal Care and Use Committee of Northwestern Polytechnical University.

Bacterial growth, enumeration and storage

LP was cultured in MRS broth at 37℃ in an incubation shaker (ZHWY-110×30, Shanghai, China). After 12 h, the probiotics were taken for subsequent experiments. It was found that there were 30–100 colonies in each plate.

LP encapsulated

The LbL encapsulation of LP was designed based on previous research and had been partially modified [22]. LP at the logarithmic growth phase was centrifuged (8000 g) for 10 min, washed three times with sterile saline, and then suspended in sterile saline to adjust its initial solubility to 1×10^{-9} (cfu/mL). CS (200 mg) was dispersed in 100 mL of 2% acetic acid and stirred for 12 h and adjust pH to 6.0. 1% (m/v) SP solution was prepared and adjust pH to 6.0. Mix 1 mL LP suspension and 40 mL CS solution evenly at room temperature, then incubate on a shaker at 100 rpm. After 30 min, the suspension was centrifuged (8000 g) at 4℃ for 10 min and washed three times with sterile saline to remove excess CS. Then add SP solution and stir thoroughly to mix evenly. At this time, the LP encapsulated with CS-SP monolayer, was obtained and named $(CS/SP)_1$-LP. Repeating this process, the $(CS/SP)_2$-LP was also obtained.

Characterization of encapsulated LP

Size and Zeta potential

The sample's size and Zeta potential were measured by Zetasizer Nano ZS (Malvern Instruments) at 25℃.

Scanning electron microscope (SEM)

The microstructure of the samples was observed using SEM. Prior to observation, the samples were subjected to vacuum. The sample was affixed to a gold-plated stainlesssteel platform using conductive adhesive, and the accelerating voltage of the scanning electron microscope was set to 20 kV.

Transmission electron microscope (TEM)

To visualize the morphology of LP and $(CS/SP)_2$-LP, TEM (HITACHI HT7800, Japan) was employed. The samples were precipitated by aspirating 10 μL drops onto a copper grid for 1 min and stained with uranyl acetate and lead citrate. The samples were then observed under TEM at an accelerating voltage of 80 kV.

Fourier transform infrared (FTIR) spectroscopy

The infrared spectra of the prepared LP, $(CS/SP)_2$-LP, CS, and SP standard samples were studied on a Nicolet iS50 FTIR spectrometer. Before FTIR analysis, all samples were dried in an electric constant temperature drying oven at 45℃ for 30 min. Scans were performed using an attenuated total reflection (ATR) device at a resolution of 4 cm^{-1} in the range of 4000 –400 cm^{-1}.

Contact angle measurement

The wetting properties of the LP, $(CS/LP)_{0.5}$-LP, $(CS/LP)_1$-LP, $(CS/LP)_{1.5}$-LP, and $(CS/SP)_2$-LP were characterized using a contact angle measurement instrument (Kruss, Hamburg, Germany).

Effect of the number of encapsulation layers on the growth of LP

Add 0.1 mL LP suspension with different numbers of encapsulation layers to 10 mL MRS broth at 37℃ in the shaker. The absorbance value of the culture at 600 nm was measured with a microplate reader every 2 h.

Survival of LP encapsulated

The survival of LP and LP encapsulated were evaluated seperately in SGF (pH 3.0) and SIF (pH 7.0). Samples were taken after LP and $(CS/SP)_2$-LP were incubated in SGF or SIF for 0, 1, 2, and 4 h separately and centrifuged (8000 g) for 5 min, washed twice with sterile saline. After diluting the suspension at gradient concentration, LP and $(CS/SP)_2$-LP were inoculated on plates in 37℃ biochemical incubator (DHP-9012, Shanghai, China) for 48 h and counted.

Gut colonization of LP encapsulated

Gastrointestinal colonization rates of probiotics following oral administration were determined in male C57BL/6 mice aged 6–8 weeks. The mice ($n=5$) were randomly grouped and provided with free access to water

and food. Mice were seperately gavaged with 0.2 mL LP and $(CS/SP)_2$-LP (1×10^8 cfu/d) for 5 days. Afterwards, the animals were sacrificed, and the contents of the stomach, small intestine and colon were collected and diluted with PBS dispersions. Each suspension (50 μL) was inoculated into solid LB medium and incubated at 37℃ for 48 h before counting.

In vivo gastrointestinal tract retention of LP encapsulated

Gastrointestinal retention of LP and $(CS/SP)_2$-LP was determined using 6-8week-old C57BL/6 mice. In order to tract the location of LP in the gastrointestinal tract, FITC was used to lable LP and its encapsulated one. After 4 h period of starvation (without food and water), each mice in one group was intragastrically administration with 1×10^8 cfu/mL of LP-FITC, while in other group it was administrated with 1×10^8 cfu/mL of $(CS/SP)_2$-LP-FITC. All mice were euthanized at predetermined time points, and their gastrointestinal fluorescence signals were captured by an animal imaging system (IVIS, Perkinelmer).

Biocompatibility

The blood from C57BL/6 mice was centrifuged at 10,000 rpm for 10 min and then washed with saline to investigate the hemolytic toxicity of LP and $(CS/SP)_2$-LP. A certain amount of saline, LP, $(CS/SP)_2$-LP, and deionized water were added to 2% mice erythrocyte saline dispersion and incubated at 37℃ for 2 h to check the stability of erythrocytes. Afterward, the mixture was centrifuged at 10,000 rpm for 15 min. The hemolysis rate was determined by measuring the absorbance of the supernatant at 545 nm using an enzyme analyzer.

Then in vivo toxicity of LP and $(CS/SP)_2$-LP was investigated using C57BL/6 male mice given 1×10^8 cfu/d of LP and $(CS/SP)_2$-LP orally for 5 consecutive days. Healthy mice treated with physiological saline were used as the control. The hearts, livers, spleens, lungs and kidneys of mice were dehydrated with 4% paraformaldehyde, embedded in paraffin, machine-cut and edge-sectioned, stained with eosin-hematoxylin (H&E), and then scanned and visualized with a tissue section scanner for observation.

Mice treatment and behavioral test

Six-month-old male AD mice were divided into 2 groups: saline-treated (APP/PS1, n=7), $(CS/SP)_2$-LP-treated (AD+$(CS/SP)_2$-LP, n=7), and saline-treated WT mice of the same month of age (WT, n=7). To assess the efficacy of $(CS/SP)_2$-LP against AD, mice were gavaged with 1×108 cfu/kg of $(CS/SP)_2$-LP daily for 6 weeks.

Open field experiment

The open-field experiments used a square box with a length, width and height of 40 cm × 40 cm × 30 cm. The box was divided into 16 square regions, contain a central region (4 square regions in the center) and a peripheral region. Each mice was placed in the same position at the beginning of the test and allowed to explore the box freely for 5 min. Their behavior was recorded and analyzed using a video tracking system (EthoVision XT, Netherlands).

Y maze experiment

The Y-maze spontaneous alternation test was used to assess spatial short-term memory and general motor activity in mice. The maze consists of three equal arms (35 cm long, 15 cm high, 5 cm wide) with an angle of 120° between them, labeled A, B, and C respectively. Each maze-naive mice were placed at the distal end of the arm labeled A, facing the center of the maze, allowed to explore the maze without interruption for 8 min and recorded. After each mice test, the experimental area was cleaned. A mice enters a maze when it enters one arm of the maze with all four paws. Alternation refers to mice entering three arms of the maze in succession. The number of alternations and the total number of arm entries were scored based on the recorded videos. The percentage of spontaneous alternations (%) was calculated as follows:

$$\%Alternation = \frac{\text{Number of Alternations}}{(\text{Total number of Arm Entries -2})} \times\ 100$$

New object recognition experiment

Novel object recognition (NOR) was used to detect the cognitive function of AD mice. During the habituation phase, each mice was allowed to freely explore an open area (40 cm × 40 cm × 30 cm) for 10 min. Each mice was placed in a box containing two identical objects (cylinders) for 10 min during the familiarization phase. Recognition memory was tested 24 h later by exposing mice to a familiar and a novel object (cylinder and sphere). After each test, all objects and equipment were cleaned with 75% ethanol to eliminate residual odors. Time spent exploring familiar objects (TF) and time spent exploring new objects (TN) were recorded and analyzed. The discrimination index (DI) is calculated as follows:

$$\text{DI} = \frac{TF}{TF+TN} \times\ 100\%$$

Morris water maze (MWM)

The MWM test used a cylindrical water tank (120 cm in diameter, 50 cm in height, and 30 cm in depth) with a video-capture system to assess spatial learning and memory abilities. The water maze pool is divided into

four quadrants. The third quadrant has a 6 cm diameter platform hidden 1 cm below the water surface. During 4 consecutive days of training, mice are trained to find the hidden platform from the starting point and the time it takes for the mice to find the platform is recorded. If the mice did not find the platform within 60 s, it was allowed to remain on the platform for 20 s. On the fifth day, the platform was removed from the tank and the mice were allowed to swim freely for 60 s, recording the number of times they traversed the platform and the amount of time they spent in the target quadrant.

Sample collection

After the behavioral experiments, all mice were euthanized by intraperitoneal injection of 0.01–0.02 mL/g sodium pentobarbital. Following this, the brains of the mice were rapidly dissected, frozen in liquid nitrogen, and stored at -80℃ for later quantitative analysis. Brain tissue and colon tissue were collected from each group of mice, fixed in 4% paraformaldehyde, and analyzed using histopathological techniques such as H&E staining, Congo red staining, Nissl staining, Thioflavin S staining, and immunofluorescence staining. In addition, the colon contents of mice were collected and stored at -80℃ for gut microbiome analysis sequencing analysis, and metabolic analysis of gut microorganisms to assess their diversity and composition.

Immunochemistry

Brain tissues were fixed with 4% paraformaldehyde for 72 h. Tissues were paraffin-embedded and sliced to 5 μm thickness and co-incubated with PSD-95 primary antibody (Servicebio, China, 1:300). After the primary antibody incubation was completed, the secondary antibody incubation was performed. A tissue section scanner was used to capture images and observe the pathological changes in the mice hippocampus.

Immunofluorescence staining

Mices brain and colon were removed, fixed with 4% paraformaldehyde, and then incubated in 30% sucrose for 72 h to dehydrate. Then, 20 μm sections were cut in a cryostat. Primary antibodies including GFAP (Shanghai Bioproducts Co., Ltd., 1:300), Iba-1 (Shanghai Bioproducts Co., Ltd., 1:300), TNF-α (Shanghai Bioproducts Co., Ltd., 1:300), IL-1β (Shanghai Bioproducts Co., Ltd., 1:300), ZO-1 (Shanghai Bioproducts Co., Ltd., 1:300), and Occludin (Shanghai Bioproducts Co., Ltd., 1:300) were applied and incubated for overnuight at 4℃. Appropriate secondary antibodies will be used for fluorescence microscope imaging.

Congo red staining

Prepare paraffin sections of brain tissue. The obtained sections were stained with Congo red. Use a tissue slice scanner to collect images and observe the Aβ deposition in the mice cortex and hippocampus.

Nissl staining

Paraffin sections of brain tissue were prepared, and the obtained brain sections were stained with cresyl violet. A tissue slice scanner was used to collect images to detect neuronal damage in the hippocampus of mice.

Thioflavin S staining

TS staining is used to label antibody plaques. Brain sections were stained with 0.002% TS (T1892-25G, Sigma-Aldrich) in 50% ethanol for 8 min in the dark and then washed twice with 50% ethanol and three times with PBS. The stained slides were observed using an orthogonal fluorescence microscope (DS-U3, Japan).

Analysis of Aβ1-42 levels in the brain by ELISA

The brain hippocampus samples were homogenized, and the concentration of $A\beta_{1\text{-}42}$ was measured using an ELISA kit (ELISA Enzyme Link, Shanghai, USA). Establish a standard curve and calculate the levels of $A\beta_{1\text{-}42}$ in tissues. The values obtained were corrected for the wet weight of the brain sample and expressed in μg/mg.

Quantitative analysis of targeted SCFAs

Collected colon contents (50 mg) were mixed with 50 μL of internal standard (5% phosphoric acid, Sigma-Aldrich), 100 μL of 125 μg/mL internal standard (isocaproic acid) solution, and 400 μL of diethyl ether. Then, SCFAs were extracted following the manufacturer's protocol (Suzhou Bionohe Gene Technology Co., Ltd., China). The obtained SCFAs samples were measured using a TRACE 1310-ISQ LT GC-MS system (Thermo Fisher, USA). The SCFAs standards were a mixture of standard acetic acid, propionic acid, isobutyric acid, butyric acid, isovaleric acid, valeric acid, and caproic acid. All standards were purchased from Sigma-Aldrich (Shanghai, China).

Gut microbiome analysis

Microbial DNA was extracted from the colon lumen of Hangzhou Lianchuang Biotechnology Co., Ltd (Hangzhou, China) using a genomic DNA kit (Omega Biotek, GA, USA) according to the operation manual. Total extracted microbial DNA was detected by agarose electrophoresis. The 16 S rDNA sequencing genes (V3-V4 region) were amplified by PCR with the addition of 341 F (5′-CCTACGGNGGCWGCAG-3′) and 805R (5′-GACTACHVGGGTATCTAATCC-3′) primers. DNA was purified with Vazyme VAHTSTM DNA Clean Beads and then quantified using the Qubit 2.0 DNA kit (Q10212,

Life Technologies Corporation, California, USA). Samples were sequenced on the Illumina NovaSeq platform LC-Bio (BioLink Inc.) provided. Characteristic abundance was normalized to the relative abundance of each sample according to the SILVA (version 138) classifier. Alpha diversity was analyzed by Chao1, Goods coverage, and Shannon's index to analyze the species diversity of the samples. Beta diversity was determined by the PCoA method.

Statistical analysis

All the data were presented as mean ± standard deviation (SD). Data were analyzed using GraphPad Prism 8 software. Significant differences between groups were determined using a two-way analysis of variance (ANOVA). Each experiment was performed at least three times.

Results

LbL encapsulated LP

CS and SP were used to encapsulate LP layer by layer (Fig. 1A). The morphology of both LP and $(CS/SP)_2$-LP was observed by SEM. As shown in Fig. 1B and C, LP appeared as an elongated rod shape with a smooth surface. After LbL encapsulation, the morphology of $(CS/SP)_2$-LP remained similar to that of LP, suggesting that LbL encapsulation did not affect the structure and morphology of LP itself. TEM images revealed a distinct nanoshell with a thickness of about 100 nm surrounding LP after encapsulation with CS and SP (Fig. 1D). Subsequent dynamic light scattering (DLS) measurements indicated changes in both size and zeta potential. During the LbL preparation process, the zeta potential of LP changed dramatically, as shown in Fig. 1E. The surface charge of LP was −16.33 ± 0.31 mV, which should attribute to its Gram-positive nature and rich content of Lipoteichoic acid (LTA) [28]. The low isoelectric point of LTA resulted in a negatively charged surface of LP, enabling it to electrostatically interact with positively charged CS. The zeta potential of $(CS/SP)_{0.5}$-LP was altered to +39.86 ± 1.07 mV, indicating the successful encapsulation of cationic CS. This value was changed to -9.69 ± 0.87 mV for $(CS/SP)_1$-LP, indicating successful encapsulation of anionic SP. Further encapsulation resulted in a zeta potential of +34.76 ± 2.53 mV for $(CS/SP)_{1.5}$-LP and 11.00 ± 0.86 mV for $(CS/SP)_2$-LP. The alternating zeta potentials confirmed the successful encapsulation of LP by LbL. Additionally, the size of encapsulated LP was larger than that of free LP, which supported the TEM results (Fig. 1F).

To demonstrate the growth and proliferation ability of $(CS/SP)_2$-LP after encapsulation, we investigated the effect of 0, 1, and 2 layers of (CS/SP) on LP growth. As shown in Fig. 1G, the growth curves of LP differed after LbL encapsulation. LP proliferated rapidly and reached the maximum proliferation about 10 h. Subsequently, growth slowed down and proliferation was inhibited. Observing the LP encapsulated with 1 or 2 layers (CS/SP), it was found that there was no growth in the first 10 h, but both the unencapsulated LP and the encapsulated LP finally reached a similar number, which shows that encapsulation has a negative impact on LP. Vitality had no significant effect. However, both unencapsulated LP and encapsulated LP eventually reached similar quantities, demonstrating that encapsulation did not significantly affect the viability of LP. The existence of proliferation stagnation could be attributed to the fact that encapsulation shields the LP from material and energy exchange with its environment. We evaluated the thermal stability performance of the encapsulated LP, revealing that LbL encapsulation enhanced the thermal stability performance of the LP (Additional file 1: Fig. S1). TGA analysis can be used to understand the changes in the material structure. As shown in Fig. S1, there are two stages of weight loss in these materials. The decomposition temperature of $(CS/SP)_2$-LP is higher than that of LP, indicating that LbL encapsulation improves the thermal stability of LP. The broad band around 3427 cm^{-1} was attributed to the stretching vibrations of -NH and -OH, as well as intermolecular and extramolecular hydrogen bonding of CS molecules (Fig. 1H). A weak band at 2872 cm^{-1} corresponded to -CH stretching. The absorption band at 1153 cm^{-1} was assigned to the asymmetric stretching of the C-O-C bridge. For the FTIR spectrum of SP, the band at 1022 cm^{-1} and the sharp peak at 1292 cm^{-1} corresponded to telescopic vibrations of $P{=}O$ and C-O, respectively. During LbL encapsulation, no new absorption peaks appeared because there was no covalent interaction between CS and SP. In addition, the -OH stretching absorption peaks were broadened between 3200 and 3700 cm^{-1} due to encapsulation, indicating that the hydroxyl group in SP formed a hydrogen bond with the amide group of CS. The contact angle of LP with different numbers of encapsulated layers was measured, and the result were shown in Fig. 1I and J. As the number of encapsulation layers increased, the contact angle of LP increased from 44.8° ± 0.9 to 51.85° ± 1.45. The results indicated that the hydrophobicity of LP increased after encapsulation, suggesting the enhanced intestinal adhesion properties if it was oral administration.

(CS/SP)2-LP gastrointestinal colonization and biocompatibility

The challenge of orally administering probiotics orally lies in their ability to survive in the gastric and intestinal fluids of the digestive tract. In order to test the resistance of $(CS/SP)_2$-LP to the gastrointestinal tract environment, simulated gastrointestinal fluids were used. As shown in Fig. 2A, after incubation in SGF for 4 h, the number of LP decreased from 5.06 log cfu/mL to 0.52 log cfu/mL,

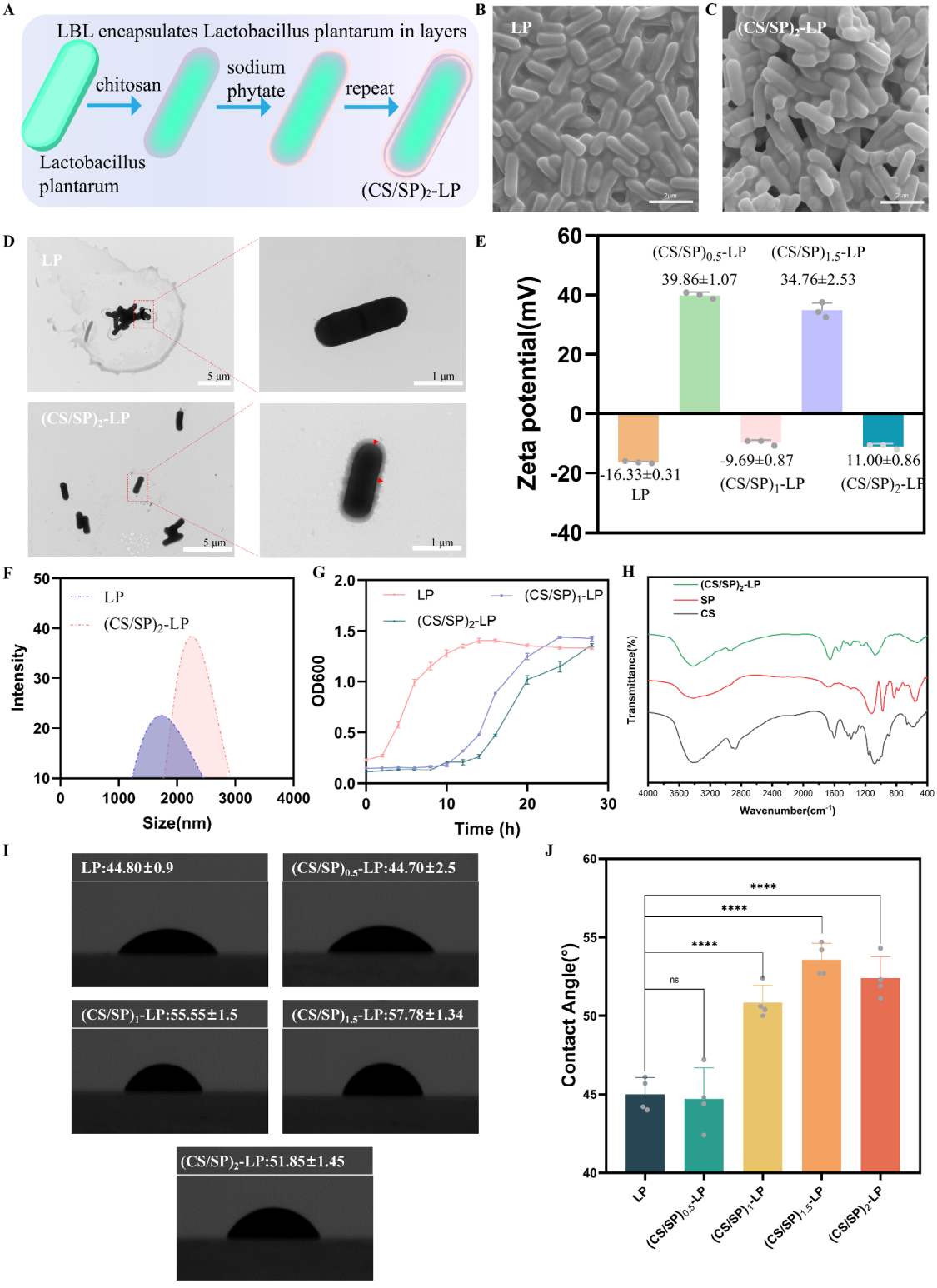

Fig. 1 Preparation and characterization of $(CS/SP)_2$-LP. (**A**) Schematic illustrating the preparation of $(CS/SP)_2$-LP using CS and SP. SEM images of (**B**) LP and (**C**) $(CS/SP)_2$-LP. Scale bar:2 μm. (**D**) Representative TEM images of LP, $(CS/SP)_2$-LP. Scale bar:1 μm. (**E**) Zeta potential of each layer during encapsulation. (**F**) Size distributions of LP and $(CS/SP)_2$-LP. (**G**) Growth curves of LP encapsulated in different layers in MRS broth ($n = 3$). (**H**) Infrared spectra of CS, SP, and $(CS/SP)_2$-LP. Indicated wettability properties of LP with different encapsulation layers. (**I**) Contact Angle Appearance. (**J**) Quantitative statistics of contact angle ($n = 4$). (ns: not statistically different, ****$p < 0.0001$)

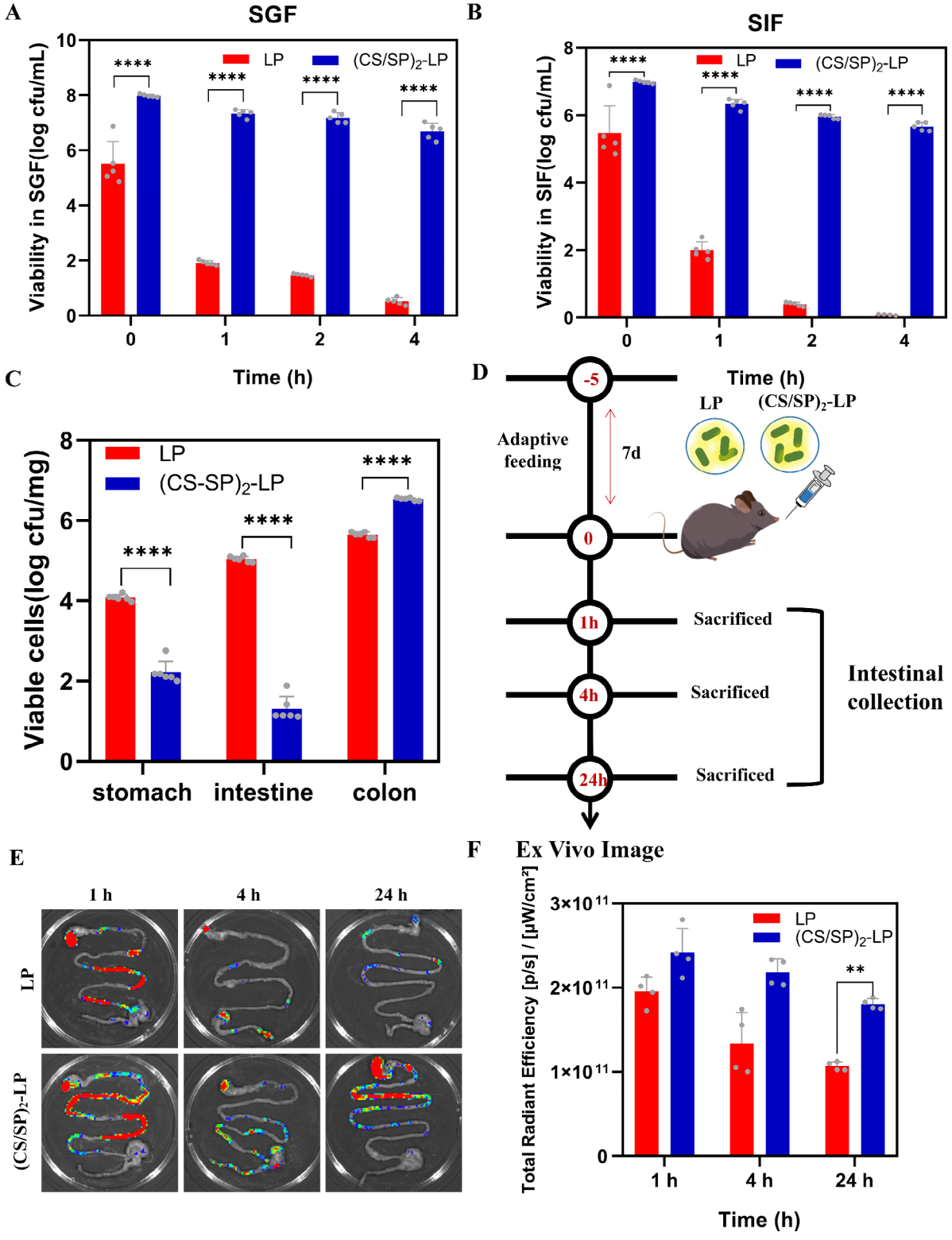

Fig. 2 Stability and retention of $(CS/SP)_2$-LP in the gastrointestinal environment. Viability count of LP and $(CS/SP)_2$-LP in SGF (**A**) and SIF (**B**) after incubation for 0, 1, 2, and 4 h ($n=5$). (**C**) Retention of probiotics in the stomach, small intestine, and colon of mice after oral administration of LP, $(CS/SP)_2$-LP ($n=6$). (**D**) Schematic diagram of the experimental schedule. (**E**) IVIS images of gastrointestinal retention of LP and $(CS/SP)_2$-LP for 1 h, 4 h, and 24 h in vivo. (**F**) IVIS images quantitative fluorescence intensity statistics ($n=4$). Results are presented as mean ± SD. ($n=4$–6, ns: no statistical difference, ****$p<0.0001$, **$p<0.01$)

whereas the number of $(CS/SP)_2$-LP only decreased from 7.94 log cfu/mL to 6.84 log cfu/mL, indicating a higher viability of $(CS/SP)_2$-LP compared to LP. A similar trend was observed for both bacteria in SIF (Fig. 2B). The strong electrostatic interactions and hydrogen bonding between the phosphate groups in SP and the amino groups in CS may prevent the diffusion of H^+ ions and bile salts into the cell wall and membrane. Thus, $(CS/SP)_2$-LP showed significant survival ability in SGF and SIF.

The retention rates of both LP and $(CS/SP)_2$-LP in the stomach, intestine, and colon were studied following oral administration to C57BL/6 mice (Fig. 2C). The preservation rates of LP were observed as follows: 28% in stomach, 34% in small intestine, 38% in colon. For $(CS/SP)_2$-LP, the low preservation rates were observed in both stomach (22%) and small intestine (13%), but a high preservation rate of 65% was observed in the colon due to the protective effect of the coating, which resulted in prolonged intestinal retention time.

The ability of probiotics to colonize in gastrointestinal tract was one of the key factors for the effectiveness of probiotic therapy. Subsequently, the distribution and intestinal colonization of LP-FITC and $(CS/SP)_2$-LP-FITC were monitored by fluorescence signal via an in vivo imaging system at different time intervals after oral administration of 1×10^8 cfu of bacteria (Fig. 2D). As shown in Fig. 2E and F, the fluorescence intensity of $(CS/SP)_2$-LP-FITC was higher than that of LP-FITC at 1 h, 4 h, and 24 h, showing the successful adherence and colonization. Quantitative analysis revealed that after 24 h of gavage, the fluorescence intensity decreased by 25% for $(CS/SP)_2$-LP compared to a decrease of 45% for LP, suggesting the improved intestinal retention time with LbL encapsulation. In conclusion, CS/SP encapsulation improved LP's gastrointestinal retention time and its intestinal colonization performance. The biocompatibility of both LP and $(CS/SP)_2$-LP was evaluated, and the results demonstrated no significant toxicity to mice, including hemolytic toxicity and histopathological analysis of major organs, such as the heart, liver, spleen, lungs, and kidneys (Additional file 1: Fig. S2-S3).

Improve cognitive and memory deficits in APP/PS1 mice by (CS/SP)2-LP treatment

In order to assess the therapeutic efficacy of $(CS/SP)_2$-LP for AD, we conducted behavioral tests on APP/PS1 transgenic mouse model to investigate its preventive effect on learning and memory impairment associated with AD. The spatial memory ability and behavioral performance of AD mice were evaluated through open-field experiments, Y maze, novel object recognition (NOR), and Morris Water Maze (MWM). The experimental protocol was illustrated in Fig. 3A. Following a two-week period of adaptive raising, the mice were divided into three groups: C57BL mice treated with saline (WT), AD mice treated with saline (APP/PS1), and AD mice treated with $(CS/SP)_2$-LP (AD+$(CS/SP)_2$-LP). All mice received continuous intragastric treatment for 6 weeks.

The results of the open-field experiment, as depicted in Fig. 3B, indicated that the mice in the WT group exhibited a greater moving distance than those in the APP/PS1 group. Furthermore, the AD mice demonstrated an increase in moving distance following $(CS/SP)_2$-LP treatment, although to a lesser extent than the untreated group. The results of the open field experiment also indicated that the mice in the WT group exhibited a faster moving speed than those in the APP/PS1 group (Fig. 3C). Furthermore, the mice in the WT group demonstrated a faster moving speed than the mice in APP/PS1 group, and despite the administration of $(CS/SP)_2$-LP to the AD mice, no significant improvement was observed. In the Y-maze experiment, the AD+$(CS/SP)_2$-LP group exhibited an increase in both spontaneous alternation rate and total number of crossings in comparison to the APP/PS1 group (Fig. 3D and E). The impact of $(CS/SP)_2$-LP treatment on spatial memory in AD mice was evaluated using NOR text. The results of the recognition index (RI) for the NOR experiment were shown in Fig. 3F. The WT group exhibited a higher RI compared to APP/PS1 group. After treatment with $(CS/SP)_2$-LP, the AD+$(CS/SP)_2$-LP group showed a significantly higher RI for novel objects compared to the APP/PS1 group, suggesting that $(CS/SP)_2$-LP treatment improved preference for novel objects and spatial memory in AD mice. Representative swimming paths of mice in the Morris water maze experiment were shown in Fig. 3H. The swimming paths of mice in the APP/PS1 group showed aimless circling, in contrast to purposeful searching for platforms by mice in the WT group and the AD+$(CS/SP)_2$-LP group. During the training trials, all groups of mice gradually learned to find hidden platforms and reduced their escape latency to reach the platform (Fig. 3G). APP/PS1 mice exhibited a longer escape latency compared to WT mice. Mice in the AD+$(CS/SP)_2$-LP group showed a shorter escape latency than the APP/PS1 group on days 3 and 4. The number of crossings over hidden platforms during spatial exploration on day 5 was presented in Fig. 3I. Mice in the APP/PS1 group had significantly fewer crossings compared with WT mice, while after $(CS/SP)_2$-LP treatment, there was a significant increase observed among AD+$(CS/SP)_2$-LP treated mice compared with those from the APP/PS1 group. Statistical results regarding time spent by mice within target quadrant were shown in Fig. 3J. Time spent by APP/PS1 mice within the target quadrant was considerably lower than that of WT mice. However, time spent within the target quadrant improved for $(CS/SP)_2$-LP treated AD modelled-mice when compared with that of untreated APP/PS1 counterparts, indicating

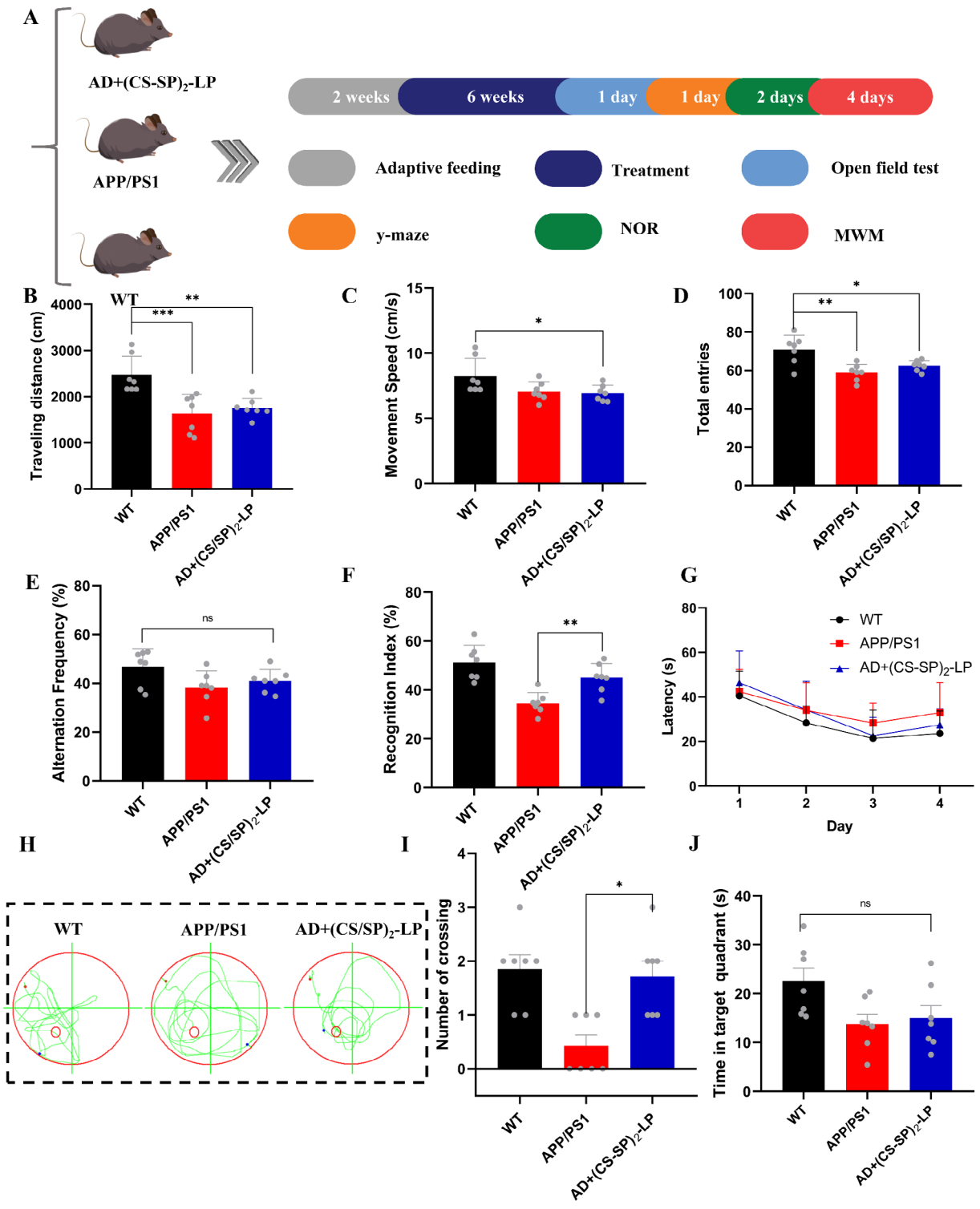

Fig. 3 Treatment with $(CS/SP)_2$-LP Improves cognitive and memory deficits in APP/PS1. (**A**) Timing scheme for drug treatment and evaluation of treatment effects in APP/PS1 mice. (**B**) Distance traveled by mice in open field experiments ($n=7$). (**C**) Movement speed of mice in open field experiments ($n=7$). (**D**) Total number of mice entries in the Y-maze experiment ($n=7$). (**E**) Spontaneous alternation rate in mice in Y-maze experiments ($n=7$). (**F**) Identifying indicators for the NOR test ($n=7$). (**G**) Escape latency of 1–4 days in mice during the MWM test in different treatment groups ($n=7$). (**H**) Representative path trajectories of mice in the MWM test ($n=7$). (**I**) Number of times crossing the hidden platform ($n=7$). (**J**) Time spent in the target quadrant ($n=7$). Results are presented as mean ± SD. (ns: no statistical difference, $^{***}p<0.001$, $^{**}p<0.01$, $^{*}p<0.05$)

an improvement of spatial learning ability impairment through $(CS/SP)_2$-LP treatment.

Effect of (CS/SP)2-LP treatment on amyloid plaques and p-Tau levels in APP/PS1 mice

To investigate the potential impact of $(CS/SP)_2$-LP on Aβ deposition in AD mice, dense amyloid plaques were visualized using Congo red staining. The number of brick-red plaques in the cortex and hippocampus was quantified in brain tissue (Fig. 4A). Notably, no brick-red plaques were observed in either the cortex or hippocampus of the WT group, while they were more prevalent in the cortex and hippocampus of APP/PS1 group compared to the WT group. However, AD+$(CS/SP)_2$-LP group exhibited significantly fewer brick-red plaques than the APP/PS1 group, indicating that treatment with $(CS/SP)_2$-LP may lead to a decrease in amyloid plaque burden. The quantity of brick-red precipitates was also measured for

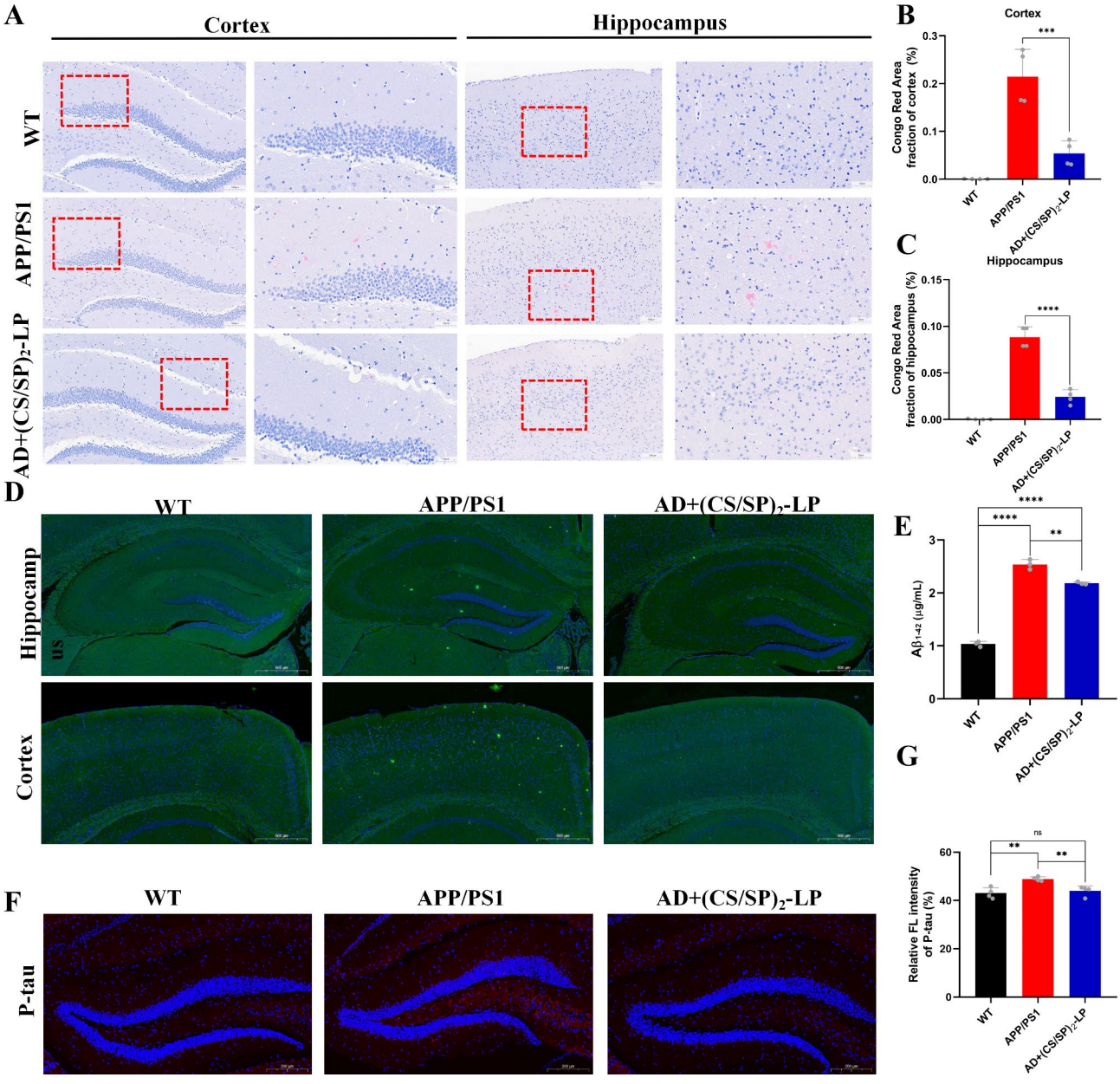

Fig. 4 Effect of $(CS/SP)_2$-LP treatment on amyloid plaques and p-Tau levels in APP/PS1 mice. (**A**) Representative photographs of Congo red staining in the cortex and hippocampus. Scale bar:100 μm. (**B-C**) Quantitative statistics of Congo red staining in cortex and hippocampus ($n = 4$). (**D**) Representative photographs of thioflavine S staining of cortical and hippocampal areas. Scale bar:500 μm. (**E**) Levels of Aβ in the brain ($n = 3$). (**F**) P-tau immunofluorescence staining of each group. Scale bar: 200 μm. P-tau (red), DAPI (blue). (**G**) Quantitative statistics of P-tau immunofluorescence staining in each group ($n = 4$). Results are presented as mean ± SD. (ns: no statistical difference, ****$p < 0.0001$, ***$p < 0.001$, **$p < 0.01$)

all three groups of mice (Fig. 4B and C). Thioflavine S staining was utilized to further examine the effect of $(CS/SP)_2$-LP treatment on Aβ deposition in AD mice brains. Figure 4D shown the results from thioflavine S staining. Significant differences were observed between the hippocampus and cortex of APP/PS1 mice with higher levels of Aβ deposition. However, this alteration was reversed by $(CS/SP)_2$-LP treatment, resulting in a significant decrease in Aβ deposition in AD mice, which was closer to that observed in WT mice. Aβ, a primary component of amyloid plaques, was quantified using an $Aβ_{1-42}$ kit to further elucidate the contribution of $(CS/SP)_2$-LP treatment in reducing the burden of Aβ in AD mice brain, as shown in Fig. 4E. The level of $Aβ_{1-42}$ in the APP/PS1 group was significantly higher than that in the WT group. However, following treatment with $(CS/SP)_2$-LP, the level decreased from 2.537 μg/mL to 2.185 μg/mL in the brains of mice. Therefore, $(CS/SP)_2$-LP treatment effectively reduced brain Aβ deposition in AD mice. The effect of $(CS/SP)_2$-LP treatment on P-tau protein was assessed through immunofluorescence staining (Fig. 4F and Additional file 1: Fig. S4). The levels of P-tau in APP/PS1 group were higher than those in WT group. However, in the AD+$(CS/SP)_2$-LP group, the levels of P-tau decreased compared to the APP/PS1 group. Quantitative analysis revealed that the fluorescence intensity of AD+$(CS/SP)_2$-LP group was similar to that of WT group (Fig. 4G). Therefore, it could be concluded that $(CS/SP)_2$-LP treatment effectively reduced Aβ deposition and tau protein phosphorylation in the brains of AD mice.

Effects of (CS/SP)2-LP treatment on neuroinflammation and synaptic proteins in APP/PS1 mice

To investigate the neurotoxicity induced by the toxic Aβ and phosphorylated tau, the histological characteristics of $(CS/SP)_2$-LP treated mice were evaluated by staining brain neuronal cells using Nissl and H&E staining [29]. As shown in 5 A and Additional file 1: Fig. S5, the results, revealed significant nuclear atrophy and neuronal damage were observed in the hippocampal regions (CA1, CA3, DG) of AD mice, while no similar phenomena were observed in the WT group. In contrast, the neuronal morphology of the brain was normalized in AD mice treated with $(CS/SP)_2$-LP. The number of neurons in the cerebral cortex and hippocampus (CA1, CA3, DG) was quantitatively analyzed. It was found that the number of neurons in the cortical area had significantly increased. The H&E staining results showed that the neurons in the brains of mice in the WT group had a good morphology and clear cell structure. In contrast, the DG area of mice in the APP/PS1 group exhibited consolidation of neuronal cells and a large number of basophilic neuronal cells. Treatment with $(CS/SP)_2$-LP reversed this change, and restored the normal neuronal structure in mice brains (Additional file 1: Fig. S6).

A substantial body of evidence suggests that soluble oligomers of Aβ and tau have the ability to propagate in various brain regions, leading directly to synaptic dysfunction and loss. Furthermore, inflammatory cytokines derived from glial cell can promote synaptic and neurotoxicity in AD [30]. PSD-95 serves as an indicator of synaptic plasticity, reflecting changes in synaptic plasticity [31]. Immunohistochemical detection was utilized to evaluate PSD-95 expression. As shown in Fig. 5A, the expression of PSD-95 was significantly lower in APP/PS1 mice compared to the WT group. In contrast, treatment with $(CS/SP)_2$-LP reversed the decrease in PSD-95 expression within in the APP/PS1 group. Quantitative analysis of PSD-95 expression in cortical and hippocampal regions revealed an increased positive area in the AD+$(CS/SP)_2$-LP group when compared to the APP/PS1 group (Additional file 1: Fig. S7). In summary, these findings demonstrate that $(CS/SP)_2$-LP treatment ameliorated abnormal synaptic plasticity in AD mice.

Microglia and astrocytes are the two primary types of glial cells in the CNS. Increasing evidence suggested that glial cells were closely associated with cognitive deficits and AD pathophysiology. Once activated, they produce various inflammatory factors that are related to neuronal death and cognitive impairment in AD [32, 33]. Immunofluorescence was used to detect the expression of ionic calcium-binding junction molecule-1 (Iba-1, microglia) and glial fibrillary acidic protein (GFAP, astrocytes). As shown in Fig. 5B and Additional file 1: Fig. S8-S9, microglia and astrocytes were strongly activated in the brains of AD mice. In contrast, $(CS/SP)_2$-LP significantly inhibited glial cell activation. The results of quantitative analysis showed similar findings (Fig. 5C and D). Glial cell activation promotes the excessive release of pro-inflammatory cytokines TNF-α and IL-1β. The pro-inflammatory cytokine TNF-α can trigger the glycogen synthase kinase-3β (GSK-3β) signaling pathway, which is mainly responsible for Aβ production and related neuroinflammation in AD [34]. IL-1β produced by activated astrocytes and microglia exacerbates tau pathology, increases Aβ deposition, impairs BBB integrity, and leads to synaptic dysfunction and neurotoxicity, causing neuroinflammation [35]. Immunofluorescence was used to analyze the expression of TNF-α and IL-1β in the brains of three groups of mice. As shown in Fig. 6A and Additional file 1: Fig. S10-S11, the overexpression of TNF-α and IL-1β in the brains of AD mice (red color) returned to normal levels after treatment with $(CS/SP)_2$-LP. These results indicated that $(CS/SP)_2$-LP effectively inhibited microglia and astrocyte activation while improving the neuroinflammatory response.

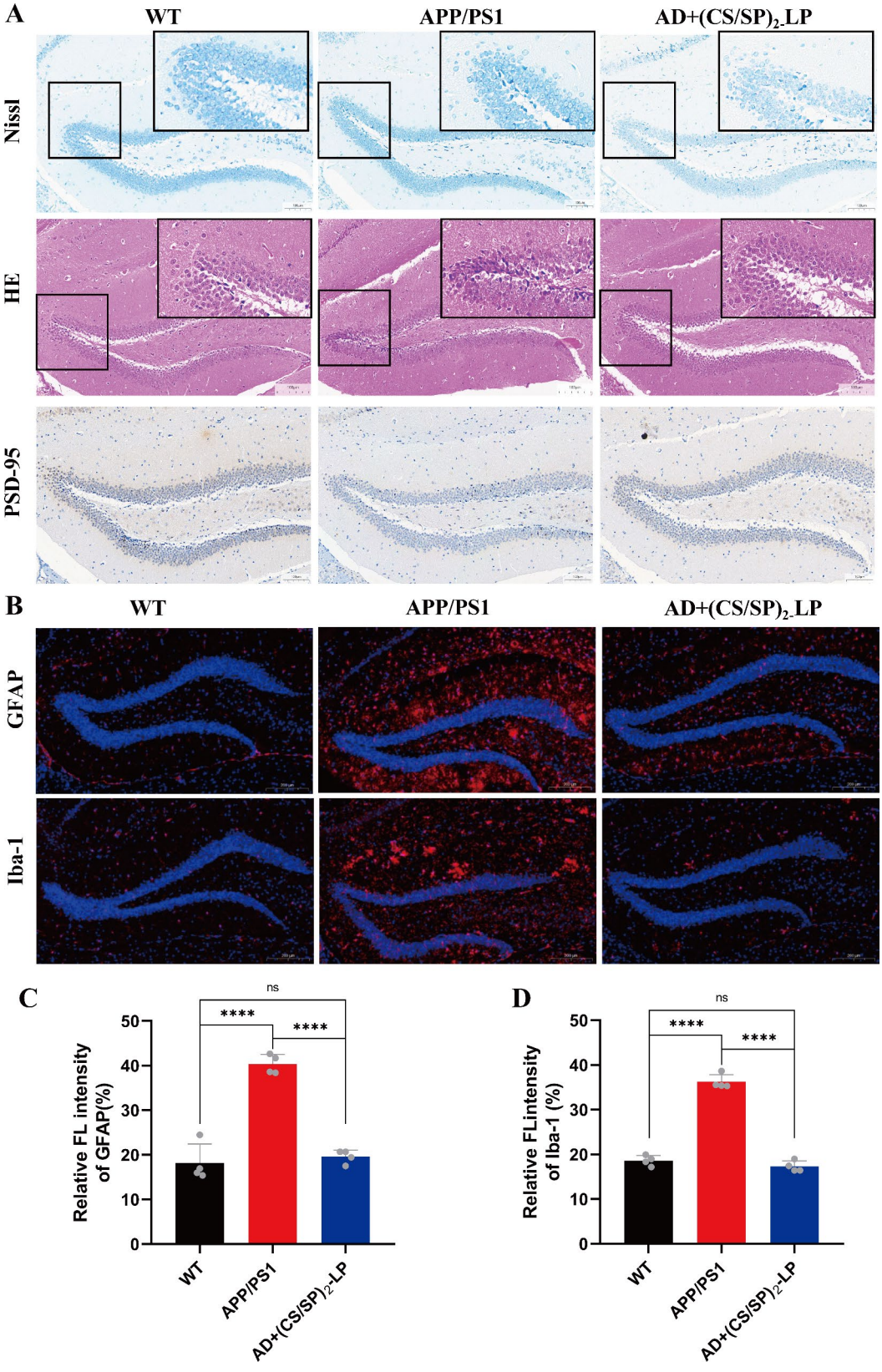

Fig. 5 Effects of $(CS/SP)_2$-LP treatment on neuroinflammation and synaptic proteins in APP/PS1 mice. (**A**) Brain tissue was stained with Nissl and H&E staining as well as PSD-95 immunofluorescence staining. Scale bar:200 μm. (**B**) Each group was stained with GFAP or Iba-1 immunofiurescence. (**C-D**) Quantitative statistics of GFAP or Ibal-1 immunofluorescence staining in each group ($n = 4$). GFAP, Iba-1(red), DAPI (blue). Results are presented as mean ± SD. (ns: no statistical difference, ****$p < 0.0001$)

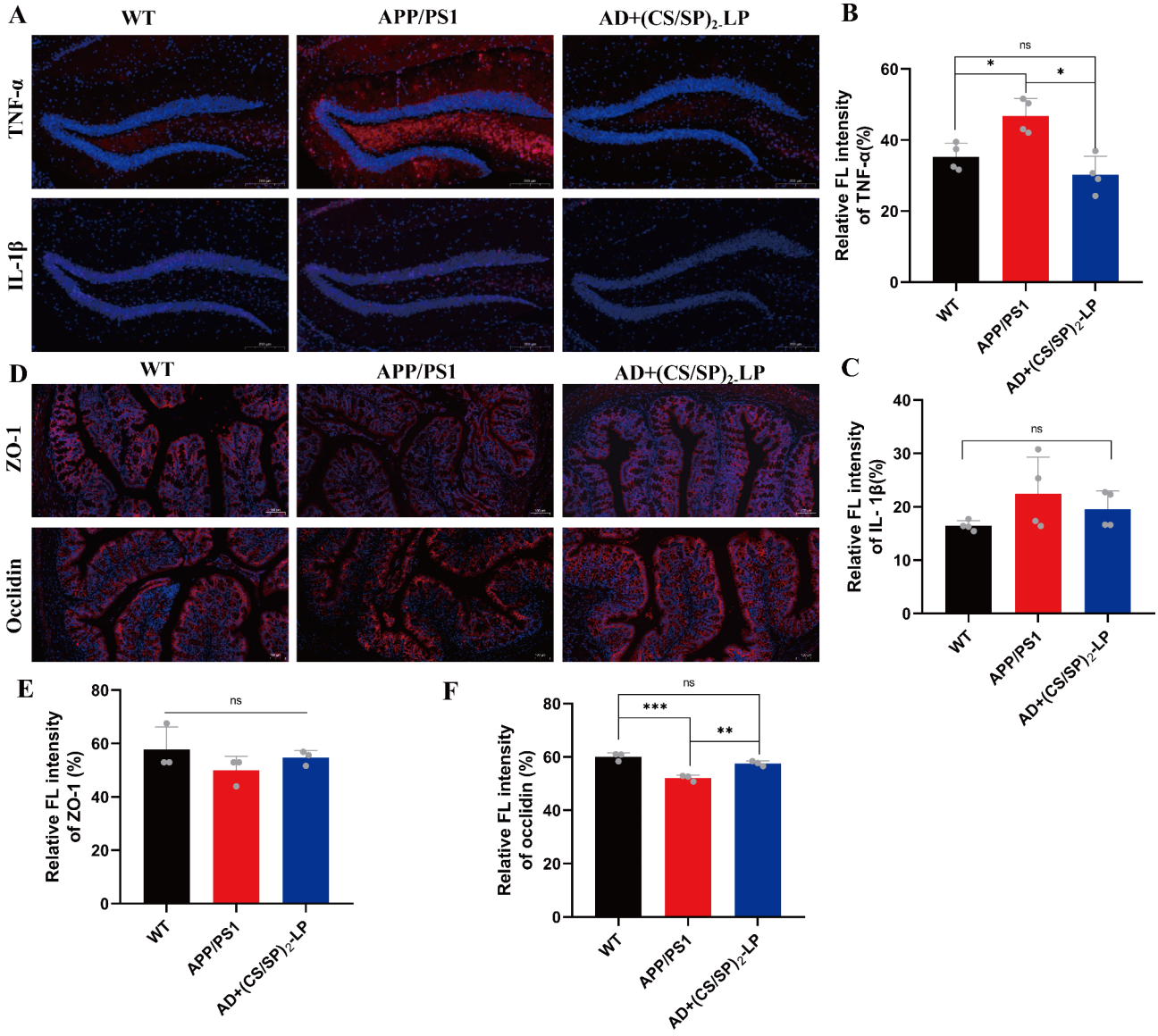

Fig. 6 Results of immunofluorescence staining were obtained for the brain proinflammatory factors TNF-α and IL-1β, as well as for the colonic tight junction-associated proteins ZO-1 and occludin. (**A**) TNF-α, IL-1βimmunofluorescence staining of each group. Scale bar: 200 μm. TNF-α, IL-1β (red), DAPI (blue). (**B-C**) Quantitative statistics of TNF-α and IL-1β immunofluorescence staining in each group ($n=4$). (**D**) ZO-1, Occludin immunofluorescence staining of each group. Scale bar: 200 μm. ZO-1, Occludin (red), DAPI (blue). (**E-F**) Quantitative statistics of ZO-1 and Occludin immunofluorescence staining in each group ($n=3$)

Effect of (CS/SP)2-LP treatment on colonic barrier integrity

Studies have demonstrated a close relationship between intestinal inflammation and the development of AD pathology [36, 37]. To investigate the potential therapeutic effects of $(CS/SP)_2$-LP on AD, we employed Immunofluorescence staining to detect the expression of tight junction-related proteins, ZO-1 and occludin, in the colon of mice. As shown in Fig. 6D and Additional file 1: Fig. S12-S13, mice in the APP/PS1 group exhibited lower levels of ZO-1 and occludin expression compared to WT group mice. However, AD mice treated with $(CS/SP)_2$-LP showed increased expressions of both proteins compared to the APP/PS1 group. H&E staining results from cross-sections of colon tissue revealed that APP/PS1 group mice had more severe damage to their colon mucosa and longer crypt lengths than those in the WT group. Nevertheless, after treatment with $(CS/SP)_2$-LP, AD mice experienced alleviated damage to their colon mucosa (Additional file 1: Fig. S14). In conclusion, treatment with $(CS/SP)_2$-LP can repair the colonic barrier and relieve mucosal damage in AD mice.

Results are presented as mean ± SD. (ns: no statistical difference, $^{***}p<0.001$, $^{**}p<0.01$, $^{*}p<0.05$).

Effect of (CS/SP)2-LP treatment on the composition of intestinal flora in APP/PS1 mice

Gut dysbiosis may play a role in the pathogenesis of AD, affecting brain function and behavior through multiple pathways in the "microbe-gut-brain" axis. These pathways include increased Aβ, phosphorylation of tau protein, neuroinflammation, metabolic dysfunction, and chronic oxidative stress [38]. To investigate the effects of $(CS/SP)_2$-LP treatment on gut microbiota in APP/PS1 mice, colonic contents were collected from each group after drug administration. 16 S rDNA gene sequencing was performed to observe the impact of $(CS/SP)_2$-LP on the gut microbiota in mice. The α-diversity index was used to evaluate microbial diversity. As shown in Fig. 7A, the Shannon index indicated that both the WT and AD+$(CS/SP)_2$-LP groups had higher community diversity. Furthermore, the AD+$(CS/SP)_2$-LP group exhibited even greater α-diversity compared to the APP/PS1 group. These findings suggested that $(CS/SP)_2$-LP played a significant role in maintaining community diversity by increasing its own α-diversity as well as overall community richness when compared to APP/PS1 mice. Additionally, when comparing Simpson indices between groups, AD+$(CS/SP)_2$-LP showed a significantly higher value than those observed for APP/PS1 mice. β-Diversity primarily serves as an evaluation tool for assessing structural and compositional differences within gut microbiota populations. Biodiversity measures based on weighted UniFrac distances displayed distinct compositions of gut microbiota between $(CS/SP)_2$-LP mice and mice in the APP/PS1 group in principal coordinate analysis (PCoA) (Fig. 7B). The utilization of Venn diagrams facilitated the examination of gut-specific (Operational Taxonomic Units) OTUs in mice among different groups. The WT group, APP/PS1 group, and AD+$(CS/SP)_2$-LP group had 150, 151, and 176 specific OTUs respectively, with a total of 159 OTUs across all three groups. Significant alterations in the composition of the gut microbiota were observed in the treatment group compared to the APP/PS1 group (Fig. 7C). Figure 7D illustrated the composition of the gut microbiota at the phylum level. The relative abundance of representative gut microbial phyla in APP/PS1 exhibited significant changes. Specifically, the relative abundance of microbiota representing gut microbiota in APP/PS1 group changed dramatically. The percentage of *Firmicutes* decreased significantly in the APP/PS1 group and the percentage of *Bacteroidetes* increased significantly in the APP/PS1 group, resulting in a decrease in the *Firmicutes*/ *Bacteroidetes* (F/B) ratio (Fig. 7E and G). However, after $(CS/SP)_2$-LP treatment, the microbiota changes in AD mice were reversed. The F/B ratio was usually considered to have a significant impact on the maintenance of intestinal homeostasis.

To identify specific bacterial taxa and compare the microbial composition of the different groups, the most abundant taxa at the genus level were identified using the ternary plot (Additional file 1: Fig. S15), and the corresponding statistical analysis was performed for several representative genera (Additional file 1: Fig. S16). Results showed that $(CS/SP)_2$-LP treatment significantly increased the abundance of *Lachnospiraceae*, *Lactobacillus*, and *HT002*, while reducing the relative abundance of *Helicobacter*. The LEfSe method was used to examine changes in the gut microbiota composition among WT, APP/PS1, and AD+$(CS/SP)_2$-LP groups to determine specific gut microbiota (LDA > 3) for each group. The $(CS/SP)_2$-LP treatment significantly affected 22 taxa, while only 17 dominant taxa were involved in APP/PS1 group. These results suggested that $(CS/SP)_2$-LP modulates the structure of mice intestinal flora and contributes to improving ecological dysregulation of intestinal flora in AD mice (Fig. 7H and I).

SCFAs analysis

Research has demonstrated that the metabolite SCFAs produced by probiotics can prevent neuronal damage by inhibiting neuroinflammation. Additionally, SCFAs have the ability to modulate the CNS and influence memory and learning processes in the brain upon entering human circulation [39]. To elucidate the regulatory effects of $(CS/SP)_2$-LP treatment on intestinal flora, we examined the content of SCFAs in colon fecal samples. The results revealed that acetic acid, propionic acid, and butyric acid were the most abundant contents in the colonic contents of the WT group (Fig. 7J). However, these SCFAs were decreased in the colons of mice in the APP/PS1 group. Specifically, compared to mice in the APP/PS1 group, mice in the WT group had 1.33 times higher acetic acid content. After $(CS/SP)_2$-LP treatment, AD mice showed a significant increase of 16.6%, 17.8%, and 52.5% respectively in acetic acid, propionic acid, and butyric acid content when compared with those in APP/PS1 group. These results suggested that $(CS/SP)_2$-LP might have a therapeutic effect by increasing SCFAs levels.

Discussion

In this study, LP was encapsulated using LbL technology to enhance its survival, retention, and colonization in the gastrointestinal tract of mice. After 6 weeks of continuous $(CS/SP)_2$-LP treatment, using APP/PS1 transgenic mice as an AD mice model, spatial memory ability was improved. Aβ deposition and tau protein phosphorylation levels decreased in the brains of AD mice. Neuronal damage was repaired, abnormal synaptic loss was improved, and the number of neurons in AD mice increased. Additionally, $(CS/SP)_2$-LP treatment repaired the colonic barrier and alleviated colonic mucosal

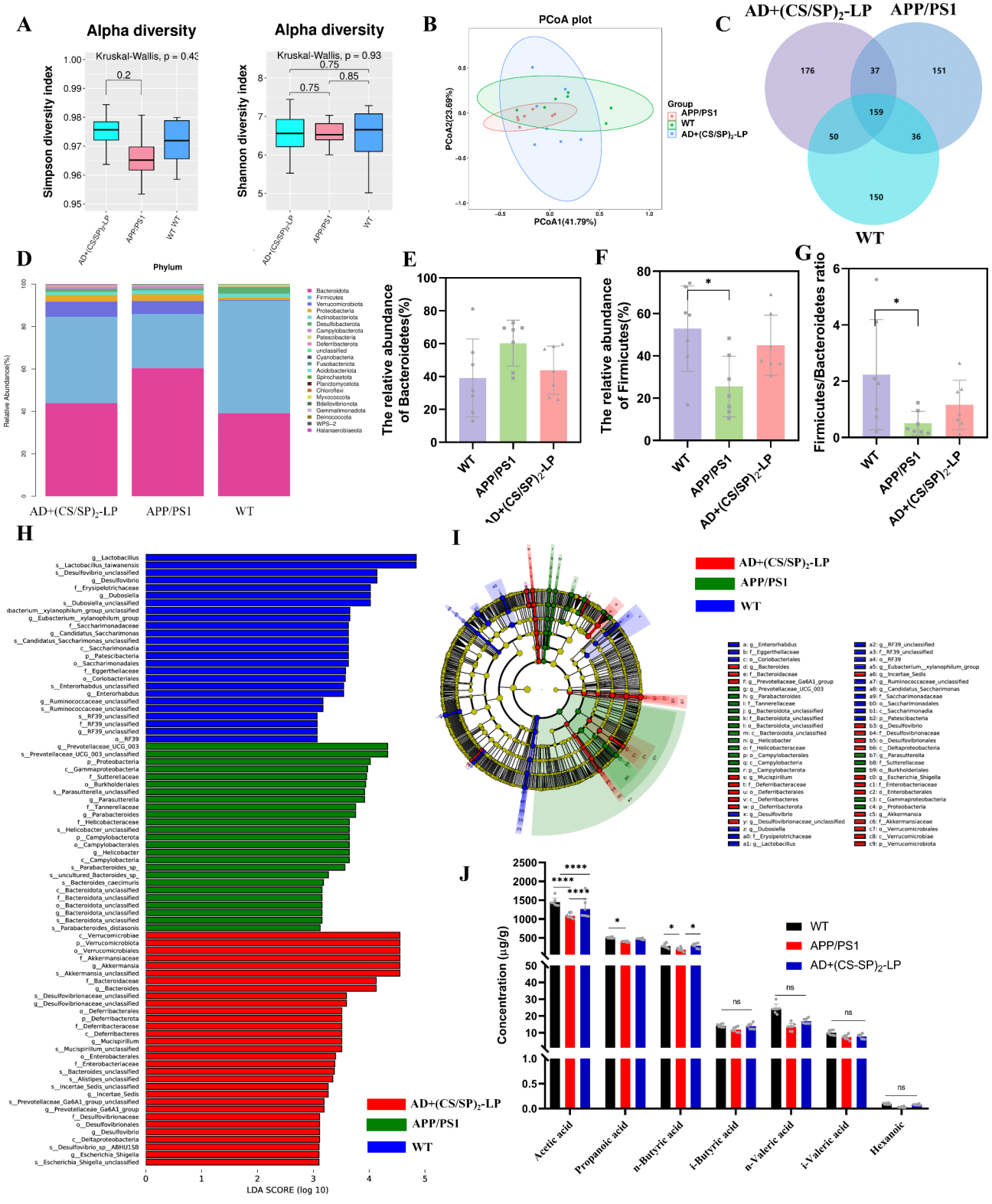

Fig. 7 Effect of $(CS/SP)_2$-LP treatment on the composition of intestinal microbiota in APP/PS1 mice. (**A**) The gut microbiota's alpha diversity was analyzed using Shannon's and Simpson's analyses. (**B**) The PCoA plot illustrates the beta diversity in different groups based on weighted UniFrac analysis. (**C**) A Venn diagram was used to show the overlap between groups. (**D**) Relative abundance of 3 groups of intestinal flora at the Phylum level. (**E**) Relative abundances of Bacteroidetes. (**F**) Relative abundances of Firmicutes. (**G**) The ratio of Firmicutes to Bacteroidetes. (**H**) LDA scores were calculated for the differentially abundant bacterial taxa among the three groups. (**I**) The cladogram was generated through LEfSe analysis. (**J**) Concentrations of SCFAs ($n = 7$). Results are presented as mean ± SD. (ns: no statistical difference, $^{****}p < 0.0001$, $^{*}p < 0.05$)

damage in AD mice. Furthermore, $(CS/SP)_2$-LP treatment increased the abundance of *Firmicutes* and elevated the content of intestinal SCFAs in AD mice.

It is hypothesized that AD symptoms might be related to the gut microbiota composition.

Increasing evidence has shown that disturbances in the gut microbiota are involved in the pathogenesis of AD. Inflammation associated with microbiota imbalance may lead to leaky gut, resulting in symptoms such as disruption of intestinal barrier integrity and increased intestinal permeability [40, 41]. The increase in intestinal permeability accompanied by intestinal bacteria, inflammatory microbial products (such as LPS), cytokine through the damaged barrier to enter the cycle, which causes systemic inflammation [42]. In addition, intestinal microorganisms are accompanied by changes in the permeability of BBB. This may cause LPS and some inflammatory factors to pass through the blood brain barrier into CNS and cause neuritis, neuron loss, neurotic damage, and eventually lead to AD [43, 44]. LPS reaches the CNS and activates astrocytes and microglia (increased Iba-1 and GFAP cells) by interacting with toll-like receptor 4 (TLR4) on the surface, thereby enhancing the expression of proinflammatory cytokines (TNF-α and IL-1β). Our results also showed that astrocytes and microglia were overactivated in the brains of AD mice compared with normal mice, and the levels of TNF-α and IL-1β were also upregulated (Fig. 5-Fig. 6). The increase in the content of proinflammatory cytokines in the brain leads to neuroinflammation locally, ultimately leading to AD. SCFAs

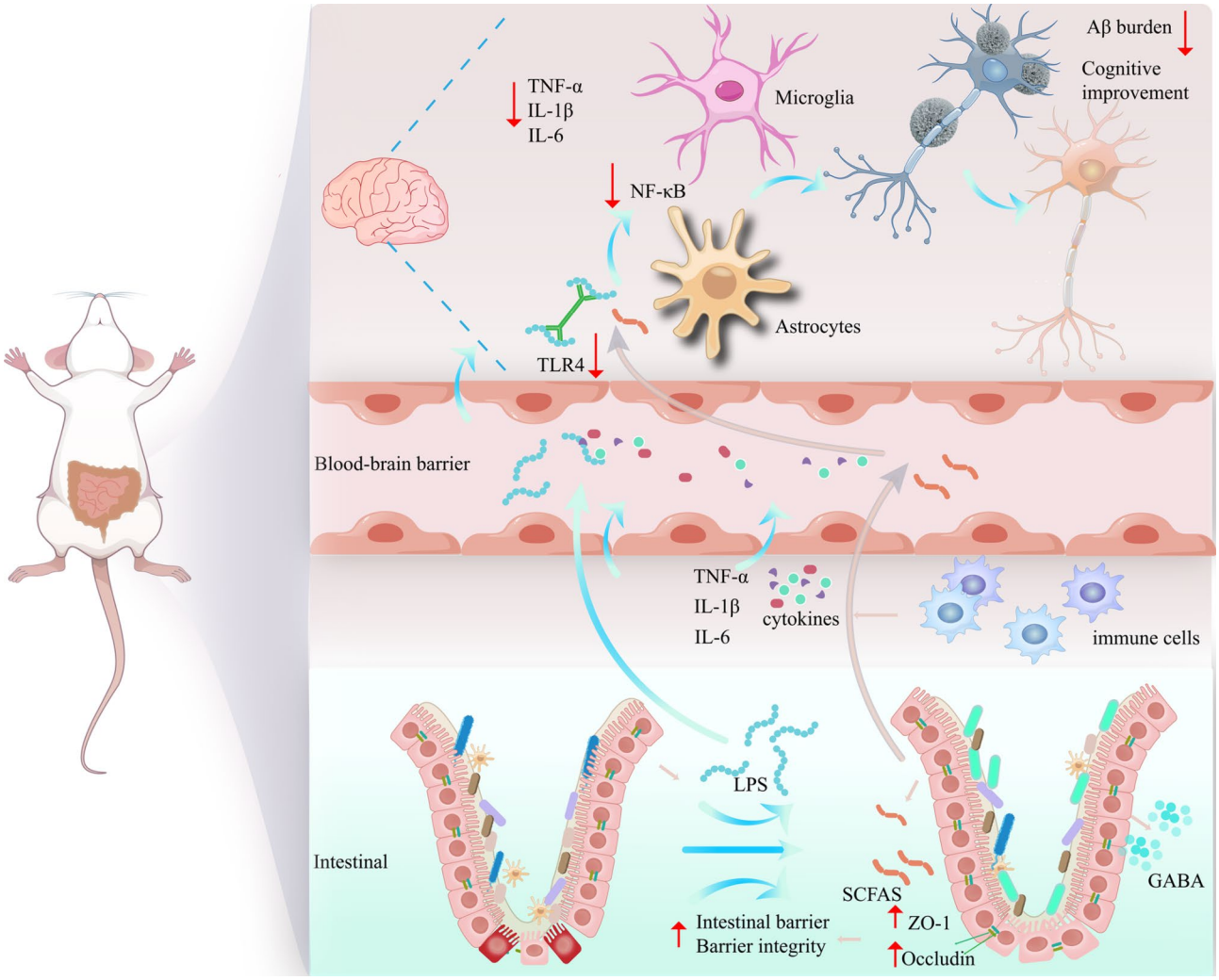

Fig. 8 Schematic diagram of the protective effects of $(CS/SP)_2$-LP on AD mouse models through the GBA. In summary, $(CS/SP)_2$-LP can significantly reduce the accumulation of Aβ in the brains of AD mice and significantly inhibit neuroinflammation and oxidative stress in the central nervous system of AD mice, indicating that $(CS/SP)_2$-LP has certain neuroprotective effect. $(CS/SP)_2$-LP treatment reshaped the intestinal microbiota of AD mice and enhanced the formation of microbial metabolite SCFAs. SCFAs enter the central nervous system through the BBB (blood-brain barrier), thereby reducing neuroinflammation in the brain by inhibiting the activation of the LPS-TLR4 signaling pathway in the central nervous system and inhibiting the excessive activation of astrocytes and microglia. and oxidative stress

has been shown to enter the BBB via the bloodstream to directly affect its integrity [45]. Studies have shown that LP ingestion can upregulate intestinal SCFAs [46, 47]. The results of this study showed that treatment with $(CS/SP)_2$-LP increased the abundance of intestinal LP in AD mice, increased the content of SCFAs, and restored intestinal permeability, thereby reducing brain Aβ burden, neuroinflammation, and neuronal damage. This may be because intestinal SCFAs can cross the blood-brain barrier, affect the integrity of the blood-brain barrier, inhibit the activation of microglia and astrocytes, and reduce neuroinflammation and Aβ accumulation in the brain (Fig. 8).

In addition, this study also has certain limitations. For example, the specific regulatory mechanism of $(CS/SP)_2$-LP in this study to improve the cognition of AD mice and reduce the Aβ burden in the brain is still unclear, and the mechanism of SCFAs improving brain neuroinflammation needs to be further clarified. In addition, the adhesion mechanism of LP in the intestinal mucosa also needs further study, in order to provide new ideas for the intestinal treatment of probiotics.

Conclusion

In summary, the use of LbL encapsulation improved the survival rate and adhesion of LP in the intestine of AD mice, breaking the limitation of probiotic treatment to gastrointestinal damage and greatly improving the therapeutic effect of probiotics. After $(CS/SP)_2$-LP treatment, the abundance of intestinal LP and the content of SCFAs in AD mice were greatly improved, and the intestinal microbiota returned to normal, and the brain neuroinflammation and Aβ burden were improved. In addition, our study showed that regulating the intestinal microbiota can improve cognitive impairment in AD patients. This study provides a new perspective for the treatment of AD.

Supplementary Information

The online version contains supplementary material available at https://doi.org/10.1186/s12951-024-02862-1.

Additional file 1: **Fig S1.** Thermal stability of LP, CS, SP, $(CS/SP)_2$-LP. **Fig S2.** Hematocompatibility of LP, $(CS/SP)_2$-LP. **Fig S3.**H&E staining of major organs such as heart, liver, spleen, lungs and kidneys in each group. **Fig S4.** Immunofluorescence staining of brain P-tau. **Fig S5.** (A) Immunohistochemical analysis of Nissl staining of neuronal cells in cortical and hippocampal areas (CA1, CA3, DG) of mice. Scale bar:100 μm. (B-E) Immunohistochemical quantitative analysis of Nissl staining of neuronal cells in mice cerebral cortex and hippocampal regions (CA1, CA3, DG) ($n=4$). Results are presented as mean ± SD. (ns: no statistical difference, $^{****}p<0.0001$, $^{***}p<0.001$, $^{*}p<0.05$). **Fig S6.** H&E staining of brain tissue in each group. **Fig S7.** Immunohistochemical staining of PSD-95 in the cerebral cortex and hippocampal area (CA1, CA3, DG) of mice in each group. **Fig S8.** GFAP immunofluorescence staining of each group. **Fig S9.** Iba-1 immunofluorescence staining of each group. **Fig S10.** Iba-1 immunofluorescence staining of each group. **Fig S11.** IL-1β immunofluorescence staining of each group. **Fig S12.** ZO-1 immunofluorescence staining of each group. **Fig S13.** Occludin immunofluorescence staining of each group. **Fig S14.** HE staining of the colon in each group. **Fig S15.** Effects of $(CS/SP)_2$-LP on microbial composition at genus levels using ternary plot method. **Fig S16.** Effects of $(CS/SP)_2$-LP on intestinal microbial composition at the genus level. order levels using ternary plot method ($n=7$).

Acknowledgements

We thank the National Natural Science Foundation of China (81803491), the Shaanxi Provincial Key R&D Program (2021SF-106, 2022SF-081), the China Postdoctoral Science Foundation (2021M702633), and the Natural Science Foundation of Shaanxi Province (Grant No. 2023-JC-YB-290)for financial support. We thank the Experimental Center of the School of Life Sciences, Northwestern Polytechnic University for supporting our research on cellular testing.

Author contributions

FFH, conceived and designed the experiments. FFH, and QG carried out the experiments. CYZ, WHZ, ZYZ, SHW contributed to analyze the experimental results. FFH and TLL wrote the manuscript. All authors reviewed the manuscript.

Data availability

No datasets were generated or analysed during the current study.

Declarations

Competing interests

The authors declare no competing interests.

Received: 27 June 2024 / Accepted: 16 September 2024
Published online: 20 September 2024

References

1. Yuan XY, Tang R, Jia Z, Chen YT, Liu J, Liu YA. Zn2+-responsive palladium nanoclusters synergistically manage Alzheimer's disease through neuroprotection and inhibition of oxidative stress. Chem Eng J 2023, 464.
2. Wang W, Zhou Q, Jiang T, Li S, Ye J, Zheng J, Wang X, Liu Y, Deng M, Ke D, et al. A novel small-molecule PROTAC selectively promotes tau clearance to improve cognitive functions in Alzheimer-like models. Theranostics. 2021;11:5279–95.
3. Zhang LX, Hou SJ, Movahedi F, Li ZJ, Li L, Hu J, Jia YB, Huang YR, Zhu J, Sun XY et al. Amyloid-beta/Tau burden and neuroinflammation dual-targeted nanomedicines synergistically restore memory and recognition of Alzheimer's disease mice. Nano Today 2023, 49.
4. Han GC, Bai KW, Yang XY, Sun CH, Ji Y, Zhou JP, Zhang HQ, Ding Y. Drug-carrier synergy therapy for amyloid-beta clearance and inhibition of tau phosphorylation via Biomimetic lipid Nanocomposite Assembly. Adv Sci 2022, 9.
5. Fu J, Li JX, Sun YZ, Liu S, Song FR, Liu ZY. In-depth investigation of the mechanisms of Schisandra chinensis polysaccharide mitigating Alzheimer's disease rat via gut microbiota and feces metabolomics. Int J Biol Macromol 2023, 232.
6. Chidambaram SB, Essa MM, Rathipriya AG, Bishir M, Ray B, Mahalakshmi AM, Tousif AH, Sakharkar MK, Kashyap RS, Friedland RP, Monaghan TM. Gut dysbiosis, defective autophagy and altered immune responses in neurodegenerative diseases: tales of a vicious cycle. Pharmacol Ther 2022, 231.
7. Lu JY, Zhang S, Huang YZ, Qian J, Tan BC, Qian XS, Zhuang J, Zou XH, Li YF, Yan FH. Periodontitis-related salivary microbiota aggravates Alzheimer's disease via gut-brain axis crosstalk. Gut Microbes 2022, 14.
8. Sun J, Xu JX, Ling Y, Wang FY, Gong TY, Yang CW, Ye SQ, Ye KY, Wei DH, Song ZQ et al. Fecal microbiota transplantation alleviated Alzheimer's disease-like pathogenesis in APP/PS1 transgenic mice. Translational Psychiatry 2019, 9.
9. Sun J, Liu SZ, Ling ZX, Wang FY, Ling Y, Gong TY, Fang N, Ye SQ, Si J, Liu JM. Fructooligosaccharides ameliorating cognitive deficits and neurodegeneration in APP/PS1 transgenic mice through modulating gut microbiota. J Agric Food Chem. 2019;67:3006–17.
10. Sun J, Xu JX, Yang B, Chen KY, Kong Y, Fang N, Gong TY, Wang FY, Ling ZX, Liu JM. Effect of Clostridium butyricum against Microglia-Mediated Neuroinflammation in Alzheimer's Disease via Regulating Gut Microbiota and Metabolites Butyrate. Mol Nutr Food Res 2020, 64.

11. Zhu GS, Zhao JX, Zhang H, Chen W, Wang G. Administration of Bifidobacterium breve improves the brain function of a beta(1–42)-Treated mice via the modulation of the gut Microbiome. Nutrients 2021, 13.
12. Yang X, Yu D, Xue L, Li H, Du J. Probiotics modulate the microbiota-gut-brain axis and improve memory deficits in aged SAMP8 mice. Acta Pharm Sinica B. 2020;10:475–87.
13. Snigdha S, Ha K, Tsai P, Dinan TG, Bartos JD, Shahid M. Probiotics: potential novel therapeutics for microbiota-gut-brain axis dysfunction across gender and lifespan. Pharmacol Ther 2022, 231.
14. Reid G, Younes JA, Van der Mei HC, Gloor GB, Knight R, Busscher HJ. Microbiota restoration: natural and supplemented recovery of human microbial communities. Nat Rev Microbiol. 2011;9:27–38.
15. Lu ZF, Zhang WQ, Zhang N, Jiang JY, Luo QZ, Qiu YM. The expression of glutamate transporters in chest compression-induced audiogenic epilepsy: a comparative study. Neurol Res. 2008;30:915–9.
16. Centurion F, Basit AW, Liu JY, Gaisford S, Rahim MA, Kalantar-Zadeh K. Nanoencapsulation for Probiotic Delivery. ACS Nano. 2021;15:18653–60.
17. Abd El-Salam MH, El-Shibiny S. Preparation and properties of milk proteins-based encapsulated probiotics: a review. Dairy Sci Technol. 2015;95:393–412.
18. Wang CY, Zhao MR, Xie JN, Wang HP, Gu ZJ, Sun FJ. Colon-targeted release of gel microspheres loaded with Antioxidative Fullerenol for Relieving Radiation-Induced Colon Injury and regulating Intestinal Flora. Adv Healthc Mater 2023.
19. Li S, Fan L, Li S, Sun X, Di Q, Zhang H, Li B, Liu X. Validation of Layer-By-Layer Coating as a Procedure to enhance Lactobacillus plantarum survival during in vitro digestion, Storage, and fermentation. J Agric Food Chem 2023.
20. Yao M, Lu Y, Zhang T, Xie J, Han S, Zhang S, Fei Y, Ling Z, Wu J, Hu Y et al. Improved functionality of ligilactobacillus salivarius Li01 in alleviating colonic inflammation by layer-by-layer microencapsulation. Npj Biofilms Microbiomes 2021, 7.
21. Han M, Lei W, Liang J, Li H, Hou M, Gao Z. The single-cell modification strategies for probiotics delivery in inflammatory bowel disease: a review. Carbohydr Polym. 2024;324:121472.
22. Anselmo AC, McHugh KJ, Webster J, Langer R, Jaklenec A. Layer-by-layer encapsulation of Probiotics for Delivery to the Microbiome. Adv Mater. 2016;28:9486–.
23. Penalva R, Martinez-Lopez AL, Gamazo C, Gonzalez-Navarro CJ, Gonzalez-Ferrero C, Virto-Resano R, Brotons-Canto A, Vitas AI, Collantes M, Penuelas I, Irache JM. Encapsulation of Lactobacillus plantarum in casein-chitosan microparticles facilitates the arrival to the colon and develops an immunomodulatory effect. Food Hydrocolloids 2023, 136.
24. Fu X, Liu Z, Zhu C, Mou H, Kong Q. Nondigestible carbohydrates, butyrate, and butyrate-producing bacteria. Crit Rev Food Sci Nutr. 2019;59:S130–52.
25. Shang Q, Jiang H, Cai C, Hao J, Li G, Yu G. Gut microbiota fermentation of marine polysaccharides and its effects on intestinal ecology: an overview. Carbohydr Polym. 2018;179:173–85.
26. Rampelli S, Candela M, Turroni S, Biagi E, Pflueger M, Wolters M, Ahrens W, Brigidi P. Microbiota and lifestyle interactions through the lifespan. Trends Food Sci Technol. 2016;57:265–72.
27. Jiang W, Peng J, Jiang N, Zhang W, Liu S, Li J, Duan D, Li Y, Peng C, Yan Y, et al. Chitosan Phytate nanoparticles: a synergistic strategy for Effective Dental Caries Prevention. ACS Nano. 2024;18:13528–37.
28. Wang MW, Yang J, Li M, Wang YF, Wu H, Xiong L, Sun QJ. Enhanced viability of layer-by-layer encapsulated < i > Lactobacillus pentosus using chitosan and sodium phytate. Food Chem. 2019;285:260–5.
29. Han GC, Bai KW, Yang XY, Sun CH, Ji Y, Zhou JP, Zhang HQ, Ding Y. Drug-carrier synergy therapy for Amyloid-β clearance and inhibition of tau phosphorylation via Biomimetic lipid Nanocomposite Assembly. Adv Sci 2022, 9.
30. Tzioras M, McGeachan RI, Durrant CS, Spires-Jones TL. Synaptic degeneration in Alzheimer disease. Nat Reviews Neurol. 2023;19:19–38.
31. Shankar GM, Li SM, Mehta TH, Garcia-Munoz A, Shepardson NE, Smith I, Brett FM, Farrell MA, Rowan MJ, Lemere CA, et al. Amyloid-beta protein dimers isolated directly from Alzheimer's brains impair synaptic plasticity and memory. Nat Med. 2008;14:837–42.
32. Lim LW, Uddin MS. Glial cells in Alzheimer?s disease: from neuropathological changes to therapeutic implications. Ageing Res Rev 2022, 78.
33. Gong YC, Huang AL, Guo X, Jia Z, Chen X, Zhu XF, Xia Y, Liu J, Xu Y, Qin XY. Selenium-core nanozymes dynamically regulates a beta & neuroinflammation circulation: augmenting repair of nervous damage. Chem Eng J 2021, 418.
34. Ly PTT, Wu Y, Zou H, Wang R, Zhou W, Kinoshita A, Zhang M, Yang Y, Cai F, Woodgett J, Song W. Inhibition of GSK3 beta-mediated BACE1 expression reduces Alzheimer-associated phenotypes. J Clin Invest. 2013;123:224–35.
35. Uddin MS, Lim LW. Glial cells in Alzheimer's disease: from neuropathological changes to therapeutic implications. Ageing Res Rev. 2022;78:101622.
36. Sochocka M, Donskow-Łysoniewska K, Diniz BS, Kurpas D, Brzozowska E, Leszek J. The gut microbiome alterations and inflammation-driven pathogenesis of Alzheimer's Disease-a critical review. Mol Neurobiol. 2019;56:1841–51.
37. Liu N, Yang C, Liang X, Cao K, Xie J, Luo Q, Luo H. Mesoporous silica nanoparticle-encapsulated Bifidobacterium attenuates brain Aβ burden and improves olfactory dysfunction of APP/PS1 mice by nasal delivery. J Nanobiotechnol. 2022;20:439.
38. Wu S, Liu X, Jiang R, Yan X, Ling Z. Roles and mechanisms of gut microbiota in patients with Alzheimer's Disease. 2021, 13.
39. Matt SM, Allen JM, Lawson MA, Mailing LJ, Woods JA, Johnson RW. Butyrate and Dietary Soluble Fiber Improve Neuroinflammation Associated With Aging in Mice. 2018, 9.
40. Obrenovich MEM. Leaky Gut, Leaky Brain? 2018;6:107.
41. Zhao Z, Ning JW, Bao XQ, Shang MY, Ma JW, Li G, Zhang D. Fecal microbiota transplantation protects rotenone-induced Parkinson's disease mice via suppressing inflammation mediated by the lipopolysaccharide-TLR4 signaling pathway through the microbiota-gut-brain axis. Microbiome 2021, 9.
42. Goyal D, Ali SA, Singh RK. Emerging role of gut microbiota in modulation of neuroinflammation and neurodegeneration with emphasis on Alzheimer's disease. Prog Neuropsychopharmacol Biol Psychiatry. 2021;106:110112.
43. Houser MC, Tansey MG. The gut-brain axis: is intestinal inflammation a silent driver of Parkinson's disease pathogenesis? Npj Parkinson's Disease. 2017;3:3.
44. Zhang W, Guo Y, Cheng Y, Yao W, Qian H. Neuroprotective effects of polysaccharide from Sparassis crispa on Alzheimer's disease-like mice: involvement of microbiota-gut-brain axis. Int J Biol Macromol. 2023;225:974–86.
45. Xie J, Bruggeman A, De Nolf C, Vandendriessche C, Van Imschoot G, Van Wonterghem E, Vereecke L, Vandenbroucke RE. Gut microbiota regulates blood-cerebrospinal fluid barrier function and Aβ pathology. EMBO J. 2023;42:e111515.
46. Nie H, Wang XX, Luo YH, Kong FH, Mu GQ, Wu XM. Mechanism explanation on improved cognitive ability of D-Gal inducing aged mice model by < i > lactiplantibacillus plantarum MWFLp-182 via the Microbiota-Gut-Brain Axis. J Agric Food Chem. 2024;72:9795–806.
47. Tang JL, Zhao MC, Chen H, Zhao BE, Wang YY, Guo YC, Wang TT, Cheng X, Ruan HR, Zhang JT, Wang HB. < i > lactiplantibacillus < i > plantarum GL001 alleviates jejunal oxidative damage induced by intestinal ischemia-reperfusion injury by influencing jejunal tissue metabolism through the improvement of jejunal microbial composition</i >. Life Sci 2023, 334.

Publisher's note